On the progress of ultrafast time-resolved THz scanning tunneling microscopy

AUTHOR(S):

Tachizaki, Takehiro; Hayashi, Kan; Kanemitsu, Yoshihiko; Hirori, Hideki

CITATION:

Tachizaki, Takehiro ...[et al]. On the progress of ultrafast time-resolved THz scanning tunneling microscopy. APL Materials 2021, 9(6): 060903.

ISSUE DATE:

2021-06

URL:

http://hdl.handle.net/2433/274565

APL Materials

On the progress of ultrafast time-resolved THz scanning tunneling microscopy

Cite as: APL Mater. **9**, 060903 (2021); https://doi.org/10.1063/5.0052051
Submitted: 29 March 2021 • Accepted: 14 May 2021 • Published Online: 01 June 2021

Takehiro Tachizaki, Kan Hayashi, Yoshihiko Kanemitsu, et al.

APL Materials PERSPECTIVE scitation.org/journal/apm

On the progress of ultrafast time-resolved THz scanning tunneling microscopy

Cite as: APL Mater. 9, 060903 (2021); doi: 10.1063/5.0052051
Submitted: 29 March 2021 • Accepted: 14 May 2021 •
Published Online: 1 June 2021

Takehiro Tachizaki,[1,a)] Kan Hayashi,[2] Yoshihiko Kanemitsu,[2] and Hideki Hirori[2,b)]

AFFILIATIONS

[1] Department of Optics and Imaging Science and Technology, Tokai University, Hiratsuka, Kanagawa 259-1292, Japan
[2] Institute for Chemical Research, Kyoto University, Uji, Kyoto 611-0011, Japan

[a)] E-mail: tachi@tokai-u.jp
[b)] Author to whom correspondence should be addressed: hirori@scl.kyoto-u.ac.jp

ABSTRACT

Scanning tunneling microscopy combined with terahertz (THz) electromagnetic pulses and its related technologies have developed remarkably. This technology has atomic-level spatial resolution in an ultrahigh vacuum and low-temperature environment, and it measures the electrical dynamical behavior of a sample's surface with femtosecond temporal resolution. In particular, it has been used to image the diffusion and relaxation dynamics of electrons in real time and real space and even instantaneously control molecular motions. In this Perspective, we focus on recent progress in research and development of ultrafast time-resolved THz scanning tunneling microscopy and its application to materials research.

I. INTRODUCTION

Since its invention in 1982,[1] scanning tunneling microscopy (STM) has been used to image the electronic states of material surfaces with atomic resolution.[2,3] In STM, electrons, driven by an applied bias voltage, pass through a tunnel junction that forms when the metallic tip is set in very close proximity to a conductive sample [Figs. 1(a) and (b)]. The resulting tunneling current varies exponentially with respect to the width of the gap w between the tip and the surface. Scanning a sample with the tip under constant bias allows us to map the topology and conductivity of the surface. When the tip is sharpened to an atomic-scale apex like in Fig. 1(a), STM is able to produce two-dimensional images of individual atoms of solid surfaces and map the local density of state (LDOS) on metallic surfaces.[4,5] STM can also be utilized as a form of spectroscopy (i.e., STS) to obtain the electrical band structure at the surface of samples.[6–10] It has been used to image the electronic states of various materials exhibiting exotic quantum properties, such as semiconductors,[11] superconductors,[6–10,12] topological insulators,[13–15] and magnetic materials.[16,17]

An enormous amount of research and development has been conducted on STM in the last 40 years; today, STM is one of the premiere tools of materials science. An important challenge has been how to obtain a fine enough time resolution to map the dynamics of materials.[18] The temporal resolution of STM had been limited by the bandwidth of the microscope's electronics (typically kHz–MHz). As a way around this limitation, ultrashort optical pulses can be irradiated on the tunnel junction as an alternative to application of an electronic bias. This method has recently been used to modulate the I–V curves transiently and measure carrier and spin dynamics with femtosecond time resolution and nanoscale spatial resolution.[19–26]

Meanwhile, the advances in the femtosecond laser have led to extensive development of spectroscopy techniques for studying various materials in the terahertz (THz) frequency region. The term "terahertz (THz) light" refers to electromagnetic waves with frequencies ranging from 0.1 to 10 THz, energies from 0.4 to 41 meV, wavelengths from 30 μm to 3 mm, and wavenumbers from 3.3 to 333 cm^{-1}.[27–29] Many elementary excitations that are distinct physical properties of solids exist in this frequency: for example, superconducting gap,[30,31] phonons,[32–34] spin resonances,[35–37] plasma frequencies,[38,39] electron binding energies of impurities,[40] and binding energies of excitons in semiconductors.[41,42] This makes the THz frequency region very attractive from the viewpoint of materials science.

In addition to the linear THz spectroscopy as mentioned above, the recent advent of technology for generating intense THz pulses

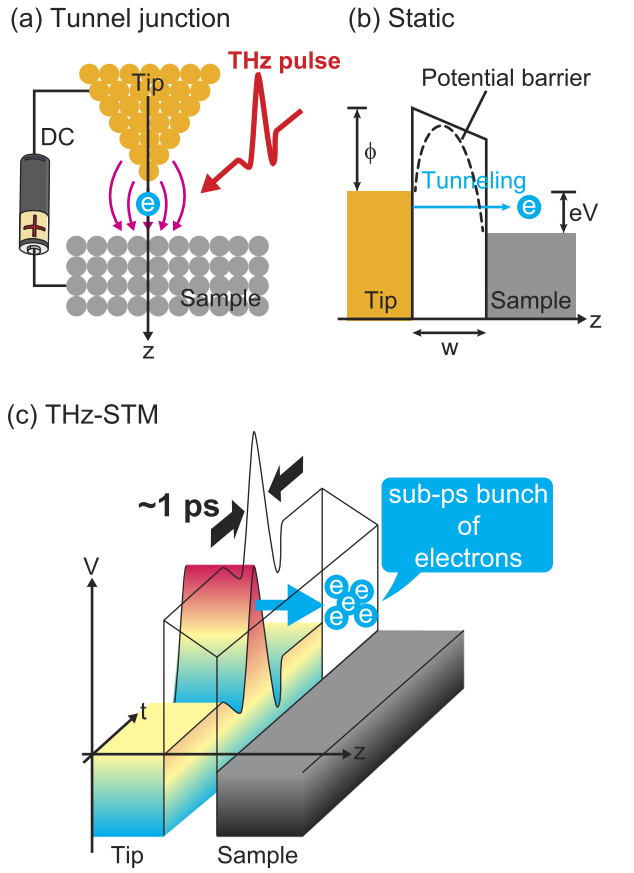

FIG. 1. Schematic diagram of tunnel junction (a) of STM biased static voltage (left half) and THz-STM (right half). (b) A potential barrier of height ϕ across an insulating layer (vacuum) of width w between the tip and sample forms the tunnel junction. The dashed line indicates the actual potential under a constant bias V. (c) The electric field accompanying the THz pulse transiently modulates the tunneling junction.

has ushered in a new era of nonlinear optics.[43–45] Now, THz pulses have started to be used as pulsed external fields for excitation and control of materials[31,33,34,36,37,41,46–52] and also have led to novel ultrafast time-resolved spectroscopic technologies with nano- and atomic-scale spatial resolutions.[20,22–24,26] It has been demonstrated that THz pulses directly modulate the potential barrier in the tunnel junction of STM and drive a transient tunneling current.[52–57] This modulation does not cause a lot of thermal energy, which would otherwise be a problem with the photoexcitation bias method. In this Perspective, we review recent progress in research and development of STM based on THz pulses.

II. FEMTOSECOND-RESOLVED DYNAMICAL IMAGING BY SCANNING TUNNELING MICROSCOPY

The energy diagram of the tunneling junction with a gap of length w under a positive bias voltage V is shown in Fig. 1(b). In this model, called the Fowler–Nordheim model,[58,59] electrons in the tip that are in energy states of the Fermi level tunnel through the barrier of height ϕ to the unoccupied energy states of the sample. Quantum mechanics tells us that the tunnel current I strongly depends on the gap length w and applied bias V: $I(V) \propto \exp(-Cw)$ [Fig. 1(b)]. The tunnel current changes exponentially with respect to the gap width w under a constant bias voltage V. The factor C in the exponential term is typically ~10 nm^{-1}, so the tunneling current varies drastically when the gap is changed by atomic-size distance. This is the fundamental principle behind STM's ability to resolve minute asperities of surfaces. This dependency is also the basis for STM's ultrahigh lateral resolution because the tunneling current is concentrated on the atom closest to the tip.

In THz-STM, the bias applied to the tunnel junction is simply from a THz pulse [Fig. 1(a)] rather than a DC voltage. The voltage arising from the irradiation varies with time [Fig. 1(c)]. The strong enhancement and spatial confinement of the THz electric field just underneath the metal tip allow the THz irradiation to be used as a local transient bias though the spot size of the THz pulse is much larger than the metal tip. In addition, because of the nonlinearity of the bias–current (I–V) relation of the tunnel junction, such a pulse causes the tip to emit a bunch of electrons that appear as a tunneling current I when the electric field reaches around the peak electric field. Thus, the temporal duration of a bunch of electrons becomes less than that of the temporal duration of the THz pulse and can reach a few hundred femtoseconds. If the applied THz pulses are single cycle or multi-cycle, the net tunnel current will be zero or very small. This is not a suitable situation for a measurement because the injected electrons generate a lot of heat that distorts the state of the sample even though the detected electric signal from these electrons may be very small. On the other hand, an asymmetric temporal shape of the THz pulse can generate a tunneling current in one direction of the electric field; because the tunneling current is unidirectional, almost all of the electrons contribute to the electrical signal. In fact, a (quasi) half-cycle THz pulse is an ideal bias for ultrafast time-resolved STM.[45]

The principle of time-resolved measurements of THz-STM is the same as in pump–probe spectroscopy. A temporally separated pair of pulses that is a combination of THz–THz[20,22,23] or THz–optical pulses[20,26] is focused on the tip–sample gap. In both cases, the tunnel current induced by THz pulse excitation is monitored as a function of the temporal separation τ between the pulses, which is varied by using an optical delay line. The THz pulse induces a tunnel current that is used as a probe of the response of the material to the optical (or THz) pump pulse. The spatial resolution of THz-STM is determined in the same way as static STM. An atomic level of resolution can be realized by appropriately setting the gap width, bias voltage, and sharpness of the apex of the tip under ultralow temperature and ultrahigh vacuum conditions.

III. DEMONSTRATIONS OF THz-STM

THz-STM was first reported by Cocker *et al.* in 2013, where it was used for imaging of highly ordered pyrolytic graphite (HOPG) and semiconductor nanodots under ambient conditions.[20] The nonlinear characteristic of the current–voltage relation (I–V curve) in the tunnel junction and bias that is the sum of the electric field of the THz pulse and DC component made an asymmetric directional tunneling current. Therefore, the THz-induced ultrashort pulsed

tunneling current appeared as a rectified current measurable with conventional electronics. This study showed that THz-STM could measure a tunnel current with 0.5 ps temporal resolution and 2 nm lateral spatial resolution.

A. Atomic resolution imaging only by applying THz-induced bias

Jelic *et al.* performed atomic-resolution imaging of the Si(111)–(7 × 7) surface by using only tunneling current induced by THz pulses.[23] Asymmetric single-cycle THz pulses were guided into an ultrahigh vacuum chamber and focused on the tip by using a polymethylpentene lens [Fig. 2(a)]. The THz pulse with a center frequency of ~0.4 THz [Fig. 2(b)] induced a transient voltage at the tunneling junction and drove a transient tunneling current [Fig. 2(c)]. The nonlinearity of the I–V relation enhanced the asymmetry of the THz induced current and generated negative current on average. This rectification model was quantitatively verified by measuring the I–V curve without and with THz pulses. The I–V curve without THz pulses showed asymmetry through the origin [Fig. 2(d), black curve]. By irradiating the tip with THz pulses, the I–V curve was shifted by −12 pA at zero bias ($V_{d.c.}$ = 0 V) without changing the overall tendency [Fig. 2(d), red curve]. The current–distance characteristic (I–z curve) was also measured when THz pulses were applied together with a DC bias and when only a DC bias was applied. The tunnel current when only DC bias was applied showed typical I–z characteristics. The overall tendency was not significantly changed even when THz pulses were added [Fig. 2(e)]. This is evidence that both the DC bias and THz pulse electric field induce a tunnel current and that the THz-induced tunnel current is inherently equivalent to the tunnel current driven by a DC bias.

THz pulse autocorrelations were used to determine the temporal resolution of THz-STM. The time delay between the THz pulse pair was controlled through a Michelson interferometer and fixed during each imaging [Fig. 2(f)]. Two-dimensional imaging of autocorrelation at constant-height STM showed the spatiotemporal localization of femtosecond tunnel current

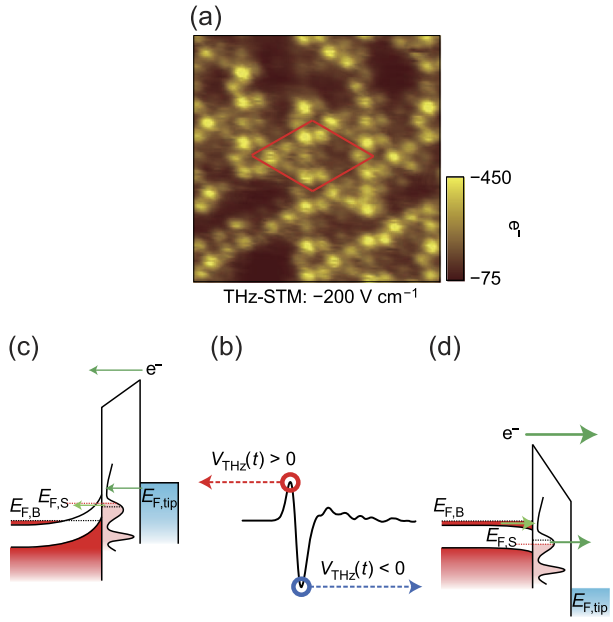

FIG. 3. Constant-height STM images of Si(111)–(7 × 7) at a THz-pulse peak electric field of −200 V/cm (a) without DC bias. Image size 9 × 9 nm^2; a 7 × 7 unit cell is shown in the red rhombus. (b) Waveform of THz pulse. (c) and (d) Band diagrams and electron flow for the first half (c) and last half (d) of the THz pulse shown in (b). The figures are reproduced from Ref. 23 with permission for the reuse of Springer Nature content.

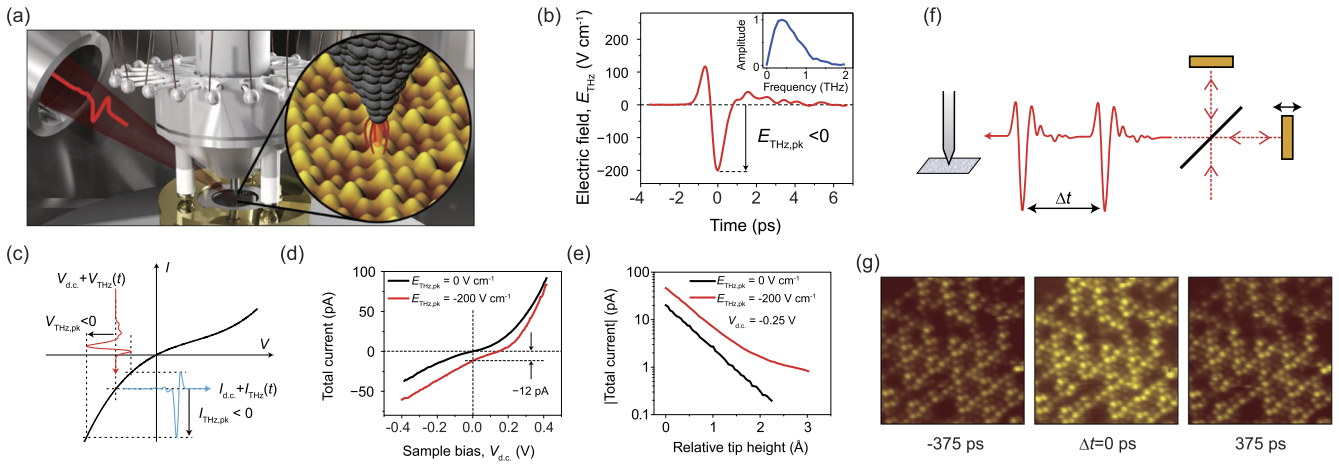

FIG. 2. (a) Schematic diagram of ultrahigh vacuum THz-STM. The inset shows the tunneling current at the junction. (b) Waveform of the THz electric field and corresponding spectrum (inset). (c) Schematic relationship between the THz-induced tunneling current (blue curve) and applied voltage (red curve). Nonlinear I–V properties (black curve) convert the temporal waveform. (d) Measured I–V curve acquired with (red curve) and without (black curve) THz pulses. (e) Measured I–z relation with (red curve) and without (black curve) THz pulses. (f) Michelson interferometer makes a pulse pair with a variable delay time Δt for autocorrelation measurements. (g) Snapshots of spatiotemporal autocorrelation obtained by the constant-height tip with an electric field of −100 V/cm for each pulse. Image size: 13 × 13 nm^2. The figures are reproduced from Ref. 23 with permission for the reuse of Springer Nature content.

[Fig. 2(g)]. These autocorrelation experiments verified the model shown in Fig. 2(c) wherein the duration of the tunnel current is shorter than the applied THz voltage because of the nonlinear I–V response.

The contrast of the THz-STM image shown in Fig. 3(a) could be explained by a model of the tunnel junction including band bending, screening, and non-equilibrium carrier occupation. A key point in this model is that the electric field of a THz pulse causes the electric band to bend across the subsurface depletion region, resulting in a shift of the surface state whose Fermi level is temporarily shifted from the bulk Fermi level. As a result, a new tunneling path through the surface states appears, and it transiently enhances the tunnel current.

As an example, let us consider a situation in which a bipolar electrical pulse with an asymmetric electric field strength is applied to the tunnel junction. The positive half cycle of the THz pulse, i.e., the first half of the pulse shown in Fig. 3(b), causes ultrafast charging of surface states by electrons tunneling from the tip. This, in turn, causes the band to bend upward and shift the surface states upward. Therefore, electrons tunnel from the tip to unoccupied states of the surface concurrently with electrons tunneling from the surface states into the unoccupied bulk states [Fig. 3(c)]. In the negative half cycle, i.e., the last half of the pulse shown in Fig. 3(b), ultrafast electron depletion of the surface states occurs until the transport of electrons from the bulk into the depletion region recovers from the band bending. During the electron depletion of the surface states, electrons on the surface tunnel to the tip and electrons in bulk move to the surface [Fig. 3(d)]. This electron flow creates more tunneling current than in the steady state because the electrons lost by the surface states due to the tunneling into the tip are continuously replenished from the bulk.

The experimental tunneling junction modulated by a picosecond transient electric field of the THz pulse was well described by a model shown above that includes the bending of the electrical band and cascading electron flow via surface states. This means that THz-STM works in the same way as static STM, even though the tunneling current induced by the THz pulse forms an ultrashort bunch of electrons. The experimental results and their interpretation showed that THz-STM is a versatile inspection apparatus with subpicosecond temporal resolution and atomic-scale spatial resolution that can be applied to various interesting materials.

B. Ultrafast carrier dynamics in C_{60} films

Spatiotemporal imaging of the diffusion dynamics of carriers was demonstrated using a C_{60} multilayer film on an Au (111) substrate.[26] The energy diagram of the sample and tunneling junction is shown in Fig. 4(a). Without optical excitation under a negative bias condition (dark condition), the tunneling current to the tip comes from the highest occupied molecular orbital (HOMO) of C_{60} that is below the Fermi surface of the Au substrate. The optical pulse (1064-nm wavelength) excites electrons in the tip and Au substrate,

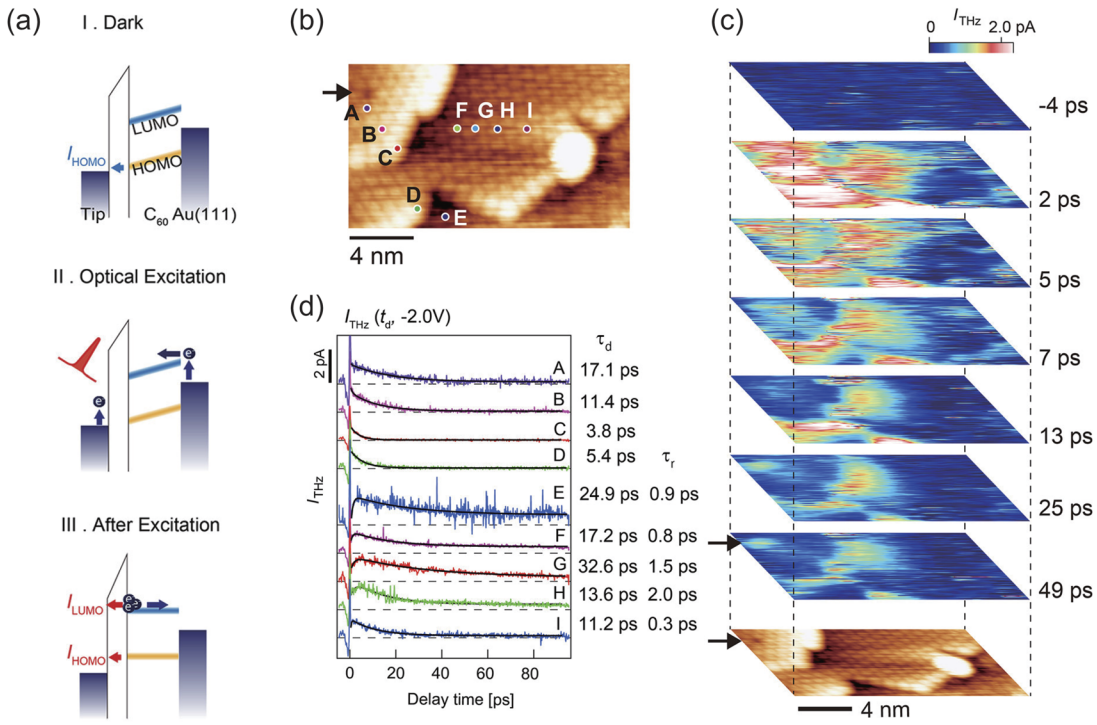

FIG. 4. (a) Band diagram of tunnel junction and schematic electron flow. (b) STM image of the C_{60} multilayer structure including steps and a vacancy defect indicated by the arrow. (c) Snapshots of tunneling currents with different delay times in the same area of (b). (d) Ultrafast tunneling currents induced by the THz pulses obtained at A to I in (b). Decay times of the tunneling currents are indicated on the right. The figures are reproduced from Ref. 26 with permission for the reuse of ACS Publications content.

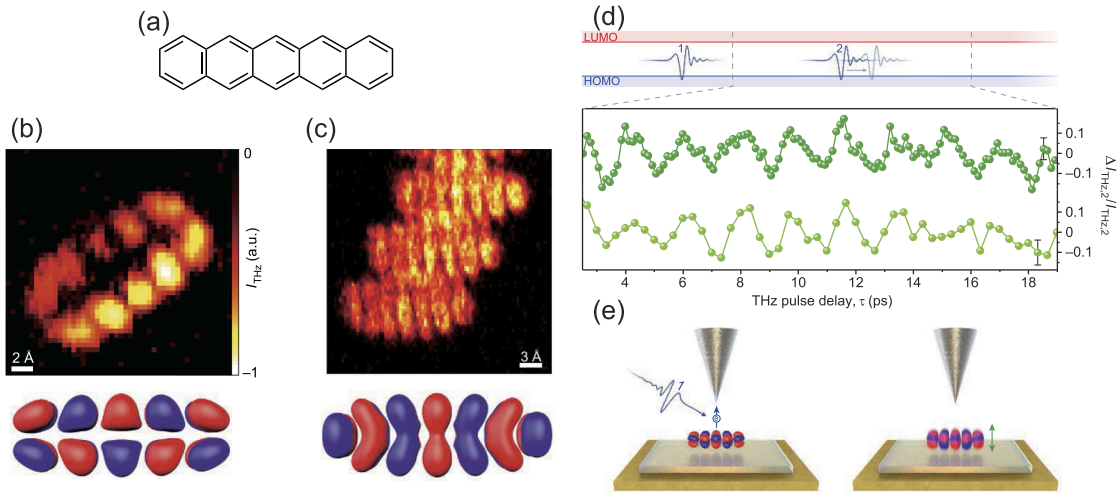

FIG. 5. (a) Molecular structure of pentacene. The THz-STM image of an isolated pentacene molecule with a maximum THz voltage set to −2.05 V (b) and +1.3 V (c). HOMO and LUMO of free pentacene simulated by DFT are illustrated at the bottom. (d) Measurement of a single pentacene molecule's dynamics in a pump and probe experiment. The tunneling current due to the second pulse (probe pulse) shows coherent oscillations as a function of delay time τ. (e) Schematic diagram of the pump and probe experiment. The first THz pulse excites a vertical vibration of the pentacene molecule by removing an electron from HOMO. The second THz pulse detects the temporal change in the heights of the molecules. The figures are reproduced from Ref. 22 with permission for the reuse of Springer Nature content.

and the electrons from the Au are injected into the lowest unoccupied molecular orbital (LUMO) of C_{60}. After the optical excitation, the tunneling current is the sum of the HOMO and LUMO. The tunneling currents via the HOMO do not change because the HOMO is always filled with electrons from the Au substrate. Therefore, the dynamical behavior of the carrier in C_{60} films is dominated by diffusion and relaxation of electrons in the LUMO.

Yoshida *et al.* clearly imaged the position-dependent temporal variation of the tunneling electrons that were injected to the LUMO of C_{60} shown in Fig. 4(b) by the optical pulses by using a single cycle THz pulse as a picosecond transient bias. The example in Fig. 4(c) shows that THz-STM can provide deep insights into materials, especially on heterogeneous surfaces that have nanoscale structures and defects. They obtained the temporal variation of the tunnel current at characteristic positions around the terrace of C_{60} including a defect. The experimental results showed that the carrier relaxation time τ strongly depends on the position of the sample structure. For example, carriers in the C_{60} molecule at the marginal of the terrace relaxed within several picoseconds [C and D in Fig. 4(d)]. On the other hand, the relaxation time becomes much longer at the middle points in the terrace [G and H in Fig. 4(b)] and near the boundary [E in Fig. 4(b)]. These results are considered to reflect the diffusivity of the electrons, the flux of the electrons to and from the surroundings, and the existence (or nonexistence) of relaxation centers, such as defects.

C. Ultrafast motion of single molecule

Cocker *et al.* used a low-temperature THz-STM to investigate an isolated pentacene adsorbed to a monolayer island of NaCl formed on an Au (110) substrate shown in Fig. 5(a).[22] Applying a combined bias consisting of a low DC voltage and THz electric field whose direction and peak strength were tuned to the resonance at the HOMO and LUMO of pentacene, the density of molecular orbits was clearly imaged [Figs. 5(b) and 5(c)] and compared with those predicted by density functional theory (DFT). In addition, the resolution of the lobes of the HOMO was sharper than in typical steady-current STM because the low-voltage bias avoided creation of artifacts. The asymmetry in the HOMO was due to the asymmetry of the tip. This high-contrast visualization of molecular orbits with a temporal resolution of 115 fs that was determined by autocorrelation measurements on pentacene shows the great potential of THz-STM.

They also monitored the motion of an isolated molecule by using constant-height THz-STM following an ultrafast excitation [Figs. 5(d) and 5(e)]. By applying a THz pulse pair with a delay time τ, they monitored the tunneling current accompanying the motion of the molecule at a temporal resolution of ~100 fs. The first THz pulse extracted the electrons from the HOMO of pentacene to the tip and then caused its vertical motion [Fig. 5(e), left]. The second THz pulse detected the height of the molecule as a change in the net tunneling current [Fig. 5(e), right]. The probe tunneling current exhibited an oscillation at a frequency of 0.5 THz [Fig. 5(d)]. They interpreted this oscillation to be a coherent vibration of the molecule and estimated its amplitude to be ±4 pm ($\pm 4 \times 10^{-12}$ m) from the tunneling currents and barrier height. In addition, they investigated other molecular vibrations in isolated pentacene and copper phthalocyanine molecules on a monolayer NaCl island formed on missing-row Au (110). This examination clarified that the molecular vibrations are governed by the van der Waals interaction between the molecule and the substrate and are coherently excited by the transient extraction of electrons by the THz pulse.

IV. SUMMARY AND PROSPECTS

As summarized above, the progress on extreme imaging techniques combining advanced THz technology with STM has been remarkable. In addition to the THz-STM technique,

time-resolved scattering-type scanning near-field optical microscopy (s-SNOM),[60–64] laser-combined angle-resolved photoemission spectroscopy (ARPES),[65,66] photoemission electron microscopy,[67–69] and time-resolved transmission electron microscopy (TR-TEM)[70–73] have high spatiotemporal and energy resolution. THz-STM will have a complementary relationship with these methods in the fields of physics, chemistry, and engineering. In particular, a static STM has been shown to be compatible with the magnetic field.[6–8] In the future, technological developments may focus on applying THz-STM to measurements in a high magnetic field for studying exotic quantum materials.

ACKNOWLEDGMENTS

The authors acknowledge the financial supports of a Grant-in-Aid for Scientific Research (Grant Nos. JP19H05824 and JP19H05465) from the Japan Society for the Promotion of Science and the Collaborative Research Program of Institute for Chemical Research, Kyoto University (Grant No. 2021-18). They also thank Tetsuo Hanaguri, Shoji Yoshida, and Hidemi Shigekwa for helpful discussions. H.H. acknowledges the financial support on this topic of the Mitsubishi Foundation, the Murata Science Foundation, and PRESTO (Grant No. JPMJPR1427) grants from Japan Science and Technology Agency.

DATA AVAILABILITY

Data sharing is not applicable to this article as no new data were created or analyzed in this study.

REFERENCES

[1] G. Binnig, H. Rohrer, C. Gerber, and E. Weibel, Phys. Rev. Lett. **49**, 57 (1982).
[2] G. Binnig, H. Rohrer, C. Gerber, and E. Weibel, Phys. Rev. Lett. **50**, 120 (1983).
[3] C. J. Chen, *Introduction to Scanning Tunneling Microscopy* (Oxford University Press, New York, 1993).
[4] Y. Hasegawa and P. Avouris, Phys. Rev. Lett. **71**, 1071 (1993).
[5] M. F. Crommie, C. P. Lutz, and D. M. Eigler, Nature **363**, 524 (1993).
[6] S. H. Pan, J. P. O'Neal, R. L. Badzey, C. Chamon, H. Ding, J. R. Engelbrecht, Z. Wang, H. Eisaki, S. Uchida, A. K. Gupta, K.-W. Ng, E. W. Hudson, K. M. Lang, and J. C. Davis, Nature **413**, 282 (2001).
[7] T. Hanaguri, C. Lupien, Y. Kohsaka, D.-H. Lee, M. Azuma, M. Takano, H. Takagi, and J. C. Davis, Nature **430**, 1001 (2004).
[8] Y. Kohsaka, C. Taylor, K. Fujita, A. Schmidt, C. Lupien, T. Hanaguri, M. Azuma, M. Takano, H. Eisaki, H. Takagi, S. Uchida, and J. C. Davis, Science **315**, 1380 (2007).
[9] Ø. Fischer, M. Kugler, I. Maggio-Aprile, C. Berthod, and C. Renner, Rev. Mod. Phys. **79**, 353 (2007).
[10] T. Machida, Y. Sun, S. Pyon, S. Takeda, Y. Kohsaka, T. Hanaguri, T. Sasagawa, and T. Tamegai, Nat. Mater. **18**, 811 (2019).
[11] F. J. Giessibl, Science **267**, 68 (1995).
[12] H. F. Hess, R. B. Robinson, R. C. Dynes, J. M. Valles, and J. V. Waszczak, Phys. Rev. Lett. **62**, 214 (1989).
[13] T. Hanaguri, K. Igarashi, M. Kawamura, H. Takagi, and T. Sasagawa, Phys. Rev. B **82**, 081305(R) (2010).
[14] P. Cheng, C. Song, T. Zhang, Y. Zhang, Y. Wang, J.-F. Jia, J. Wang, Y. Wang, B.-F. Zhu, X. Chen, X. Ma, K. He, L. Wang, X. Dai, Z. Fang, X. Xie, X.-L. Qi, C.-X. Liu, S.-C. Zhang, and Q.-K. Xue, Phys. Rev. Lett. **105**, 076801 (2010).
[15] Y.-S. Fu, M. Kawamura, K. Igarashi, H. Takagi, T. Hanaguri, and T. Sasagawa, Nat. Phys. **10**, 815 (2014).
[16] R. Wiesendanger, Rev. Mod. Phys. **81**, 1495 (2009).
[17] S. Loth, M. Etzkorn, C. P. Lutz, D. M. Eigler, and A. J. Heinrich, Science **329**, 1628 (2010).
[18] R. J. Hamers and D. G. Cahill, Appl. Phys. Lett. **57**, 2031 (1990).
[19] Y. Terada, S. Yoshida, O. Takeuchi, and H. Shigekawa, Nat. Photonics **4**, 869 (2010).
[20] T. L. Cocker, V. Jelic, M. Gupta, S. J. Molesky, J. A. J. Burgess, G. D. L. Reyes, L. V. Titova, Y. Y. Tsui, M. R. Freeman, and F. A. Hegmann, Nat. Photonics **7**, 620 (2013).
[21] S. Yoshida, Y. Aizawa, Z.-h. Wang, R. Oshima, Y. Mera, E. Matsuyama, H. Oigawa, O. Takeuchi, and H. Shigekawa, Nat. Nanotechnol. **9**, 588 (2014).
[22] T. L. Cocker, D. Peller, P. Yu, J. Repp, and R. Huber, Nature **539**, 263 (2016).
[23] V. Jelic, K. Iwaszczuk, P. H. Nguyen, C. Rathje, G. J. Hornig, H. M. Sharum, J. R. Hoffman, M. R. Freeman, and F. A. Hegmann, Nat. Phys. **13**, 591 (2017).
[24] D. Peller, L. Z. Kastner, T. Buchner, C. Roelcke, F. Albrecht, N. Moll, R. Huber, and J. Repp, Nature **585**, 58 (2020).
[25] M. Garg and K. Kern, Science **367**, 411 (2020).
[26] S. Yoshida, Y. Arashida, H. Hirori, T. Tachizaki, A. Taninaka, H. Ueno, O. Takeuchi, and H. Shigekawa, ACS Photonics **8**, 315 (2021).
[27] M. Tonouchi, Nat. Photonics **1**, 97 (2007).
[28] P. U. Jepsen, D. G. Cooke, and M. Koch, Laser Photonics Rev. **5**, 124 (2011).
[29] R. Ulbricht, E. Hendry, J. Shan, T. F. Heinz, and M. Bonn, Rev. Mod. Phys. **83**, 543 (2011).
[30] M. Dressel and G. Grüner, *Electrodynamics of Solids: Optical Properties of Electrons in Matter* (Cambridge University Press, Cambridge, UK, 2002).
[31] R. Matsunaga, N. Tsuji, H. Fujita, A. Sugioka, K. Makise, Y. Uzawa, H. Terai, Z. Wang, H. Aoki, and R. Shimano, Science **345**, 1145 (2014).
[32] M. Nagai, T. Tomioka, M. Ashida, M. Hoyano, R. Akashi, Y. Yamada, T. Aharen, and Y. Kanemitsu, Phys. Rev. Lett. **121**, 145506 (2018).
[33] X. Li, T. Qiu, J. Zhang, E. Baldini, J. Lu, A. M. Rappe, and K. A. Nelson, Science **364**, 1079 (2019).
[34] F. Sekiguchi, H. Hirori, G. Yumoto, A. Shimazaki, T. Nakamura, A. Wakamiya, and Y. Kanemitsu, Phys. Rev. Lett. **126**, 077401 (2021).
[35] T. Kampfrath, A. Sell, G. Klatt, A. Pashkin, S. Mährlein, T. Dekorsy, M. Wolf, M. Fiebig, A. Leitenstorfer, and R. Huber, Nat. Photonics **5**, 31 (2011).
[36] Y. Mukai, H. Hirori, T. Yamamoto, H. Kageyama, and K. Tanaka, Appl. Phys. Lett. **105**, 022410 (2014).
[37] Y. Mukai, H. Hirori, T. Yamamoto, H. Kageyama, and K. Tanaka, New J. Phys. **18**, 013045 (2016).
[38] R. Huber, F. Tauser, A. Brodschelm, M. Bichler, G. Abstreiter, and A. Leitenstorfer, Nature **414**, 286 (2001).
[39] R. A. Kaindl, M. A. Carnahan, D. Hägele, R. Lövenich, and D. S. Chemla, Nature **423**, 734 (2003).
[40] Y. Mukai, H. Hirori, and K. Tanaka, Phys. Rev. B **87**, 201202 (2013).
[41] H. Hirori, M. Nagai, and K. Tanaka, Phys. Rev. B **81**, 081305(R) (2010).
[42] K. Uchida, T. Otobe, T. Mochizuki, C. Kim, M. Yoshita, H. Akiyama, L. N. Pfeiffer, K. W. West, K. Tanaka, and H. Hirori, Phys. Rev. Lett. **117**, 277402 (2016).
[43] J. Hebling, G. Almási, I. Kozma, and J. Kuhl, Opt. Express **10**, 1161 (2002).
[44] K.-L. Yeh, M. C. Hoffmann, J. Hebling, and K. A. Nelson, Appl. Phys. Lett. **90**, 171121 (2007).
[45] H. Hirori, A. Doi, F. Blanchard, and K. Tanaka, Appl. Phys. Lett. **98**, 091106 (2011).
[46] H. Hirori, K. Shinokita, M. Shirai, S. Tani, Y. Kadoya, and K. Tanaka, Nat. Commun. **2**, 594 (2011).
[47] M. Liu, H. Y. Hwang, H. Tao, A. C. Strikwerda, K. Fan, G. R. Keiser, A. J. Sternbach, K. G. West, S. Kittiwatanakul, J. Lu, S. A. Wolf, F. G. Omenetto, X. Zhang, K. A. Nelson, and R. D. Averitt, Nature **487**, 345 (2012).
[48] Y. Sanari, T. Tachizaki, Y. Saito, K. Makino, P. Fons, A. V. Kolobov, J. Tominaga, K. Tanaka, Y. Kanemitsu, M. Hase, and H. Hirori, Phys. Rev. Lett. **121**, 165702 (2018).
[49] T. Kampfrath, K. Tanaka, and K. A. Nelson, Nat. Photonics **7**, 680 (2013).
[50] H. Hirori and K. Tanaka, J. Phys. Soc. Jpn. **85**, 082001 (2016).
[51] C. Schmidt, J. Bühler, A.-C. Heinrich, J. Allerbeck, R. Podzimski, D. Berghoff, T. Meier, W. G. Schmidt, C. Reichl, W. Wegscheider, D. Brida, and A. Leitenstorfer, Nat. Commun. **9**, 2890 (2018).

[52]K. Yoshioka, I. Katayama, Y. Minami, M. Kitajima, S. Yoshida, H. Shigekawa, and J. Takeda, Nat. Photonics **10**, 762 (2016).
[53]K. Yoshioka, I. Katayama, Y. Arashida, A. Ban, Y. Kawada, K. Konishi, H. Takahashi, and J. Takeda, Nano Lett. **18**, 5198 (2018).
[54]M. Ludwig, G. Aguirregabiria, F. Ritzkowsky, T. Rybka, D. C. Marinica, J. Aizpurua, A. G. Borisov, A. Leitenstorfer, and D. Brida, Nat. Phys. **16**, 341 (2020).
[55]S. Yoshida, H. Hirori, T. Tachizaki, K. Yoshioka, Y. Arashida, Z.-H. Wang, Y. Sanari, O. Takeuchi, Y. Kanemitsu, and H. Shigekawa, ACS Photonics **6**, 1356 (2019).
[56]D. Peller, C. Roelcke, L. Z. Kastner, T. Buchner, A. Neef, J. Hayes, F. Bonafé, D. Sidler, M. Ruggenthaler, A. Rubio, R. Huber, and J. Repp, Nat. Photonics **15**, 143 (2021).
[57]M. Abdo, S. Sheng, S. Rolf-Pissarczyk, L. Arnhold, J. A. J. Burgess, M. Isobe, L. Malavolti, and S. Loth, ACS Photonics **8**, 702 (2021).
[58]R. H. Fowler and L. Nordheim, Proc. R. Soc. London, Ser. A **119**, 173 (1928).
[59]J. G. Simmons, J. Appl. Phys. **34**, 1793 (1963).
[60]K. Karki, M. Namboodiri, T. Zeb Khan, and A. Materny, Appl. Phys. Lett. **100**, 153103 (2012).
[61]M. Eisele, T. L. Cocker, M. A. Huber, M. Plankl, L. Viti, D. Ercolani, L. Sorba, M. S. Vitiello, and R. Huber, Nat. Photonics **8**, 841 (2014).
[62]M. Wagner, Z. Fei, A. S. McLeod, A. S. Rodin, W. Bao, E. G. Iwinski, Z. Zhao, M. Goldflam, M. Liu, G. Dominguez, M. Thiemens, M. M. Fogler, A. H. Castro Neto, C. N. Lau, S. Amarie, F. Keilmann, and D. N. Basov, Nano Lett. **14**, 894 (2014).
[63]S. A. Dönges, O. Khatib, B. T. O'Callahan, J. M. Atkin, J. H. Park, D. Cobden, and M. B. Raschke, Nano Lett. **16**, 3029 (2016).
[64]M. Mrejen, L. Yadgarov, A. Levanon, and H. Suchowski, Sci. Adv. **5**, eaat9618 (2019).
[65]T. Kiss, T. Shimojima, K. Ishizaka, A. Chainani, T. Togashi, T. Kanai, X.-Y. Wang, C.-T. Chen, S. Watanabe, and S. Shin, Rev. Sci. Instrum. **79**, 023106 (2008).
[66]I. Gierz, J. C. Petersen, M. Mitrano, C. Cacho, I. C. E. Turcu, E. Springate, A. Stöhr, A. Köhler, U. Starke, and A. Cavalleri, Nat. Mater. **12**, 1119 (2013).
[67]A. Kubo, K. Onda, H. Petek, Z. Sun, Y. S. Jung, and H. K. Kim, Nano Lett. **5**, 1123 (2005).
[68]K. Fukumoto, Y. Yamada, K. Onda, and S.-y. Koshihara, Appl. Phys. Lett. **104**, 053117 (2014).
[69]M. K. L. Man, A. Margiolakis, S. Deckoff-Jones, T. Harada, E. L. Wong, M. B. M. Krishna, J. Madéo, A. Winchester, S. Lei, R. Vajtai, P. M. Ajayan, and K. M. Dani, Nat. Nanotechnol. **12**, 36 (2017).
[70]P. Baum, D.-S. Yang, and A. H. Zewail, Science **318**, 788 (2007).
[71]T. Ishikawa, S. A. Hayes, S. Keskin, G. Corthey, M. Hada, K. Pichugin, A. Marx, J. Hirscht, K. Shionuma, K. Onda, Y. Okimoto, S.-y. Koshihara, T. Yamamoto, H. Cui, M. Nomura, Y. Oshima, M. Abdel-Jawad, R. Kato, and R. J. D. Miller, Science **350**, 1501 (2015).
[72]S.-i. Ideta, D. Zhang, A. G. Dijkstra, S. Artyukhin, S. Keskin, R. Cingolani, T. Shimojima, K. Ishizaka, H. Ishii, K. Kudo, M. Nohara, and R. J. D. Miller, Sci. Adv. **4**, eaar3867 (2018).
[73]T. Danz, T. Domröse, and C. Ropers, Science **371**, 371 (2021).